Developmental Cell
Article

DRE-1/FBXO11-Dependent Degradation of BLMP-1/BLIMP-1 Governs *C. elegans* Developmental Timing and Maturation

Moritz Horn,[1,2] Christoph Geisen,[1] Lukas Cermak,[4,5] Ben Becker,[1] Shuhei Nakamura,[1] Corinna Klein,[1] Michele Pagano,[4,5] and Adam Antebi[1,2,3,*]
[1]Max Planck Institute for Biology of Ageing, Joseph-Stelzmann-Straße 9b, 50931 Cologne, Germany
[2]Cologne Excellence Cluster on Cellular Stress Responses in Aging Associated Diseases (CECAD), University of Cologne, 50674 Cologne, Germany
[3]Department of Molecular and Cellular Biology, Huffington Center on Aging, Baylor College of Medicine, Houston, TX 77030, USA
[4]Department of Pathology, NYU Cancer Institute, New York University School of Medicine, 522 First Avenue, SRB 1107, New York, NY 10016, USA
[5]Howard Hughes Medical Institute, Department of Pathology, NYU Cancer Institute, New York University School of Medicine, 522 First Avenue, SRB 1107, New York, NY 10016, USA
*Correspondence: aantebi@age.mpg.de
http://dx.doi.org/10.1016/j.devcel.2014.01.028

SUMMARY

Developmental timing genes catalyze stem cell progression and animal maturation programs across taxa. *Caenorhabditis elegans* DRE-1/FBXO11 functions in an SCF E3-ubiquitin ligase complex to regulate the transition to adult programs, but its cognate proteolytic substrates are unknown. Here, we identify the conserved transcription factor BLMP-1 as a substrate of the $SCF^{DRE-1/FBXO11}$ complex. *blmp-1* deletion suppressed *dre-1* mutant phenotypes and exhibited developmental timing defects opposite to *dre-1*. *blmp-1* also opposed *dre-1* for other life history traits, including entry into the dauer diapause and longevity. BLMP-1 protein was strikingly elevated upon *dre-1* depletion and dysregulated in a stage- and tissue-specific manner. The role of DRE-1 in regulating BLMP-1 stability is evolutionary conserved, as we observed direct protein interaction and degradation function for worm and human counterparts. Taken together, posttranslational regulation of BLMP-1/BLIMP-1 by DRE-1/FBXO11 coordinates *C. elegans* developmental timing and other life history traits, suggesting that this two-protein module mediates metazoan maturation processes.

INTRODUCTION

All metazoans develop via successive life stages and mature to reproductive adults. At the cellular level, temporal and positional fates must be precisely regulated to ensure coordination of proliferative, morphogenetic, and differentiation events. The nematode *Caenorhabditis elegans* develops from embryo, through four larval stages, to reach reproductive maturity. Each larval stage is marked by ecdysis and characterized by virtually invariant patterns of stage-specific cellular events (Sulston and Horvitz, 1977).

Temporal selectors called heterochronic genes orchestrate temporal cellular fates during *C. elegans* larval development across tissues (Ambros and Horvitz, 1984). Mutations in the heterochronic loci result in precocious or retarded expression of stage-specific cellular events, which often manifest as a deletion or repetition of such programs. There are over 30 identified heterochronic loci, which encode various transcriptional, translational, and posttranslational regulators (Resnick et al., 2010). Importantly, most heterochronic genes are highly conserved and have emerged as crucial regulators of proliferation, differentiation, and stem cell dynamics in mammals (Rybak et al., 2009; Yu et al., 2007). For example, the RNA binding protein LIN28 has been implicated in precocious puberty in humans (Park et al., 2012), revealing remarkable conservation of function from the molecular to the organismal level.

C. elegans dre-1 was isolated in an enhancer screen for DAF-12/FXR/VDR-redundant functions in gonadal heterochrony, as the double mutant gives rise to a synthetic gonadal migration defect in which the gonadal arms fail to turn on schedule (Fielenbach et al., 2007). On their own, *dre-1* hypomorphic mutants also display heterochronic phenotypes in epidermal stem cells, called seams, causing precocious seam cell fusion and terminal differentiation a full stage earlier than normal (Fielenbach et al., 2007). *dre-1* null mutants arrest after hatching or in the L1 stage often displaying molting defects.

F box proteins function as the substrate-recognition components of SKP1-CUL1-F box (SCF) E3-ubiquitin ligase complexes, thus conferring substrate specificity to the ubiquitin-proteasome system (UPS) (Skaar et al., 2013). *C. elegans* DRE-1 and its mammalian homolog FBXO11 are F box proteins and have previously been shown to work in an SCF complex (Duan et al., 2012; Fielenbach et al., 2007). Interestingly, DRE-1/FBXO11 is one of only about ten F box proteins highly conserved across all major taxa (Shaye and Greenwald, 2011).

In mice, homozygous mutation of *Fbxo11* results in facial cleft-ing and perinatal lethality, as observed in *Mutt* and *Jeff* mutant mice, which were identified in ENU mutagenesis screens. Moreover, in mice and humans, *Fbxo11* haploinsufficiency is linked to the onset of otitis media, an inflammation of the middle ear

affecting children (Hardisty et al., 2003; Hardisty-Hughes et al., 2006; Segade et al., 2006). Two substrates of human FBXO11, BCL6 and CDT2, which promote lymphoma formation and delay cell-cycle exit, respectively, have recently been identified (Abbas et al., 2013; Duan et al., 2012; Rossi et al., 2013). However, the substrates mediating developmental timing alterations in *dre-1/Fbxo11* mutants have remained largely elusive.

To elucidate the mechanism of posttranslational control of developmental timing by DRE-1/FBXO11, we sought to identify proteolytic targets by performing genetic suppressor screens in *C. elegans*. We discovered that the highly conserved zinc-finger transcriptional repressor BLMP-1/BLIMP-1 is regulated by the $SCF^{DRE-1/FBXO11}$ complex via proteasome-dependent degradation. Our studies reveal that *blmp-1* is a heterochronic gene, whose misregulation accounts for most developmental alterations observed in *dre-1* mutants and demonstrate that DRE-1-dependent BLMP-1 regulation is conserved across taxa.

RESULTS

blmp-1 and *nhr-25* Suppress *dre-1* Epidermal Heterochrony

Because DRE-1/FBXO11 acts as the substrate-recognition component of an SCF E3-ubiquitin ligase complex, we reasoned that *dre-1* loss of function would lead to aberrant accumulation of client substrates. If so, then knockdown of such substrates should suppress the developmental timing defects seen in *dre-1* mutants. We therefore performed an RNAi-based suppressor screen, looking for amelioration of developmental timing defects in partial loss-of-function *dre-1(dh99)* mutants. We focused our screen initially on transcription factors as well as known heterochronic loci as candidates. We identified the zinc-finger transcription factor *blmp-1* as a potent suppressor of *dre-1* heterochronic phenotypes. The predicted *C. elegans* BLMP-1 protein harbors an N-terminal SET domain, a proline-rich domain, and five paired-domain zinc fingers at the C terminus. An existing deletion allele *tm548* lacks part of exon 3 and results in a frameshift that disrupts the SET domain and all subsequent zinc fingers, suggesting it is a null allele. Mammalian BLIMP-1 is the major B-lymphocyte maturation factor but also governs various cell-fate decisions, including primordial germ cell specification and skin differentiation, generally working as a transcriptional repressor (Horsley et al., 2006; Ohinata et al., 2005; Turner et al., 1994). Importantly, *C. elegans* BLMP-1 and mammalian BLIMP-1 show high domain conservation, with 43% similarity in the SET domain and 70% similarity in the zinc fingers (Tunyaplin et al., 2000).

blmp-1 loss of function suppressed *dre-1* phenotypes in multiple tissues, including epidermis and gonad. During normal terminal differentiation of the hypodermis, epidermal seam cells exit the cell cycle early in the L4 larval stage, fuse, and then synthesize a continuous ridged cuticular structure called adult alae (Figure 1A). In *dre-1* partial loss-of-function mutants (e.g., *dre-1(dh99)*) seam cells undergo precocious terminal differentiation in L3, a full stage ahead of schedule (Fielenbach et al., 2007) (Figures 1A–1C). Using the adherens junction marker *ajm-1:gfp* to mark seam cell boundaries, we observed that *blmp-1* knockdown by RNAi reduced *dre-1(dh99)* precocious seam cell fusion from 90% to 15% of the animals (Figures 1B and 1C). Similarly only 7.5% of *dre-1;blmp-1(tm548)* double mutant animals showed seam cell fusion in L3 (Figure 1C). Notably, *blmp-1* mutants themselves displayed heterochronic phenotypes: although *blmp-1* mutants had normal timing for seam cell division and fusion (Table S1 available online), they exhibited incomplete adult alae synthesis, a phenotype typical of weakly retarded mutants (Figures 1D and 1E). Incomplete alae formation was rescued by introducing a fosmid-based *blmp-1::gfp* translational fusion construct (Figure 1E), demonstrating that the phenotype arises from lesions in *blmp-1*. Moreover, in *dre-1;blmp-1* double mutants, the incomplete alae formation phenotype of *blmp-1* prevailed, placing *blmp-1* genetically downstream (Figures 1A and 1E). Thus, *blmp-1* and *dre-1* have opposite phenotypes in the seams, and *dre-1* phenotypes depend on functional *blmp-1(+)*.

Another transcription factor identified in our screen was the homolog of mammalian steroidogenic-factor-1, called *nhr-25*, a nuclear hormone receptor implicated in *C. elegans* molting and epidermal developmental timing (Gissendanner and Sluder, 2000; Hada et al., 2010; Silhánková et al., 2005). Notably, *nhr-25* depletion reportedly induces retarded seam cell fusion and prevents precocious adult alae formation (Hada et al., 2010). We observed that *nhr-25* depletion also significantly suppressed *dre-1* precocious seam cell fusion from 90% to 21.5% of the animals (Figure 1C). Thus, complete terminal differentiation of *C. elegans* epidermal stem cells depends on both *blmp-1* and *nhr-25*.

blmp-1 Suppresses *dre-1* Gonadal Heterochrony

We next asked whether *blmp-1* and *nhr-25* also influenced *dre-1* developmental timing phenotypes in the gonad. In hermaphrodites, gonadal morphogenesis is led by two distal tip cells (dtcs), which migrate from midbody in opposite directions toward head and tail during L2. In L3, dtcs reflex dorsally and centripetally back toward the midbody to form two U-shaped gonadal arms in adult animals (Figure 2A). Whereas *dre-1* mutants on their own show only a weakly retarded gonadal migration phenotype, combinations with other heterochronic loci, such as *daf-12*/FXR/VDR or the *lin-29*/EGR null mutants, unveil a strongly synthetic retarded phenotype in which both gonadal arms fail to reflex (Figures 2A–2C) (Fielenbach et al., 2007). The unreflexed gonadal phenotype is interpreted as a reiteration of L2-programs, with concomitant prevention of L3-specific gonadal events.

Strikingly, depletion of *blmp-1* suppressed the strongly retarded phenotype of *dre-1(dh99);daf-12(rh61rh411)* mutants, restoring the dorsal turn in more than 80% of the animals (Figures 2B and 2C). In contrast, *nhr-25* knockdown failed to suppress the gonadal migration defect (Figure 2C). *blmp-1* depletion also restored gonadal reflection in *dre-1;lin-29(n546)* mutants, whereas gonadal migration defects in *daf-12;lin-29* remained unaffected (Figure 2C). These observations reveal that *blmp-1* specifically suppresses gonadal heterochronic phenotypes arising from *dre-1* mutation, and not *daf-12* or *lin-29* mutation, suggesting that *dre-1* and *blmp-1* work in a unified pathway. Consistent with a role in gonadal developmental timing, *blmp-1* mutants on their own showed precocious gonadal migration defects; dtcs navigated the first turn dorsally 2–3 hr ahead of schedule but often failed the second turn and continued migration toward head and tail (Figures 2A, 2D, and 2E). These phenotypes were rescued by the full-length *blmp-1::gfp* transgene (Figure 2E). Notably, the early gonadal migration defect prevailed in *dre-1;daf-12* mutants

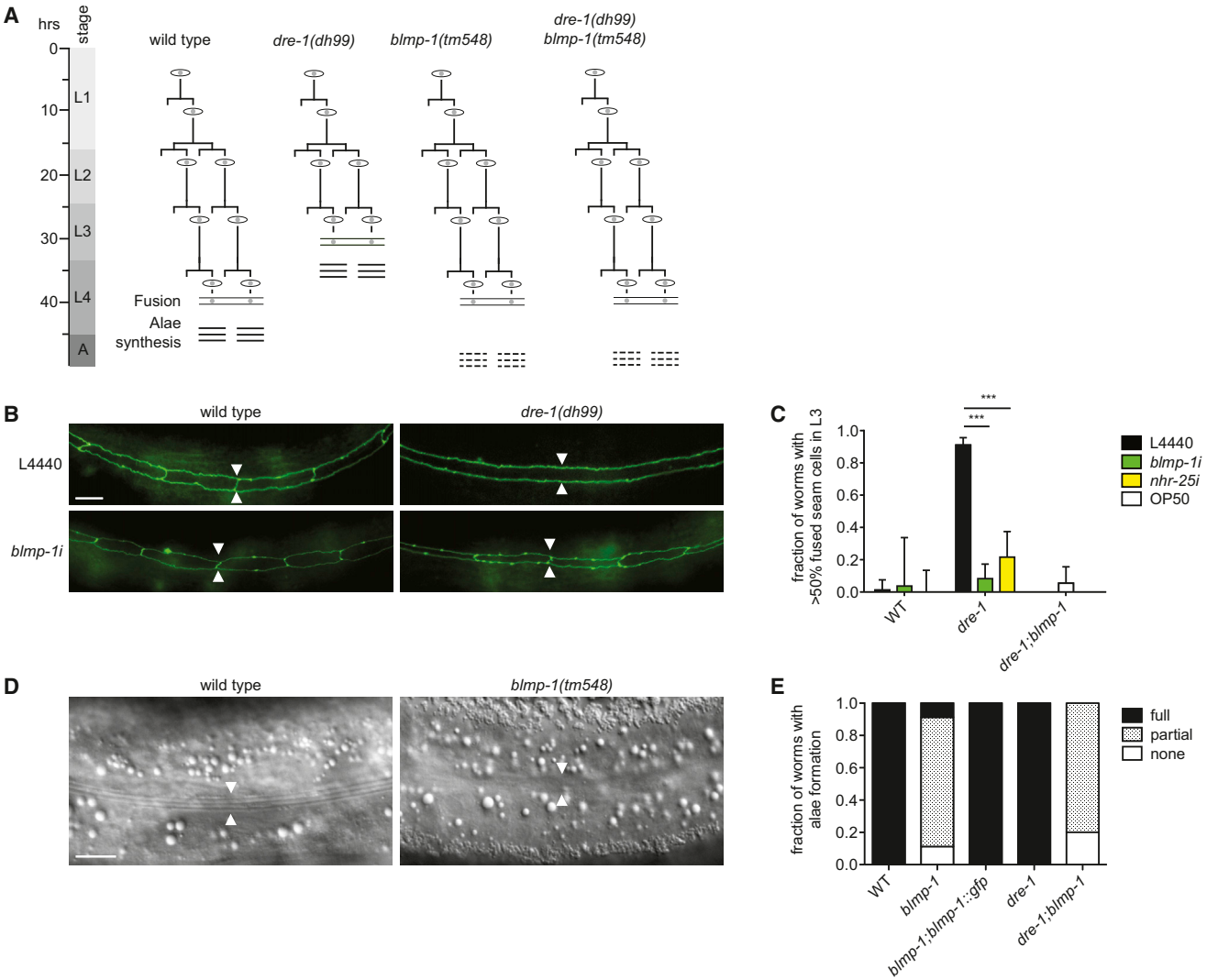

Figure 1. *blmp-1* Promotes Terminal Differentiation in the Hypodermis

(A) Seam cell lineages from WT worms and various mutants as inferred from inspection. Terminal differentiation is indicated by fusion of the seams (eye-shaped cells) and adult alae formation (three horizontal bars). *dre-1* mutants exhibit precocious seam cell terminal differentiation, whereas *blmp-1* and the double mutants show incomplete formation of adult alae (three dashed horizontal bars).

(B) Representative images of seam cell adherence junctions as visualized by *ajm-1::gfp* in WT and *dre-1* L3 larvae grown on L4440 empty vector control or *blmp-1* RNAi, respectively. Arrowheads indicate seam-seam boundaries.

(C) *blmp-1* and *nhr-25* RNAi suppress *dre-1* precocious seam cell fusion in L3 larvae. ***$p < 0.001$ (Fisher's exact test). Mean + 95% CI ($n > 30$).

(D) Representative DIC images of young adult WT and *blmp-1* mutant worms. Arrowheads indicate seam cell positions.

(E) *blmp-1* and *dre-1;blmp-1* mutants show poor formation of adult alae. The *blmp-1* mutant phenotype is rescued by a *blmp-1::gfp* transgene ($n > 20$).

Scale bars, 10 μm (B and D).

See also Table S1.

grown on *blmp-1* RNAi (Figures 2A and 2E), consistent with *blmp-1* acting downstream of *dre-1*. Taken together, these results show that *dre-1*/*blmp-1* also function together to coordinate temporal patterning of gonadal outgrowth. Because *blmp-1*, and not *nhr-25*, suppressed *dre-1* phenotypes in multiple tissues, we focused our further analyses on *blmp-1*.

blmp-1 Works Late in the Heterochronic Circuit

To further elucidate the role of *blmp-1* in the seam cell heterochronic circuit, we first performed genetic epistasis experiments with precocious heterochronic loci that work at the larval-to-adult switch. Among them, *hbl-1*/Hunchback, *lin-42*/Period, *lin-41*/Trim71, and *sop-2*/PolycombG-like specify L4 programs by preventing *lin-29*/EGR expression and thus the adult fate (Abrahante et al., 2003; Cai et al., 2008; Rougvie and Ambros, 1995; Slack et al., 2000; Tennessen et al., 2006). Loss-of-function mutants typically show impenetrant precocious terminal differentiation, in which seam cells fuse and synthesize adult alae precociously in L3 larvae. Knockdown of *blmp-1* variously suppressed precocious seam cell phenotypes of these mutants,

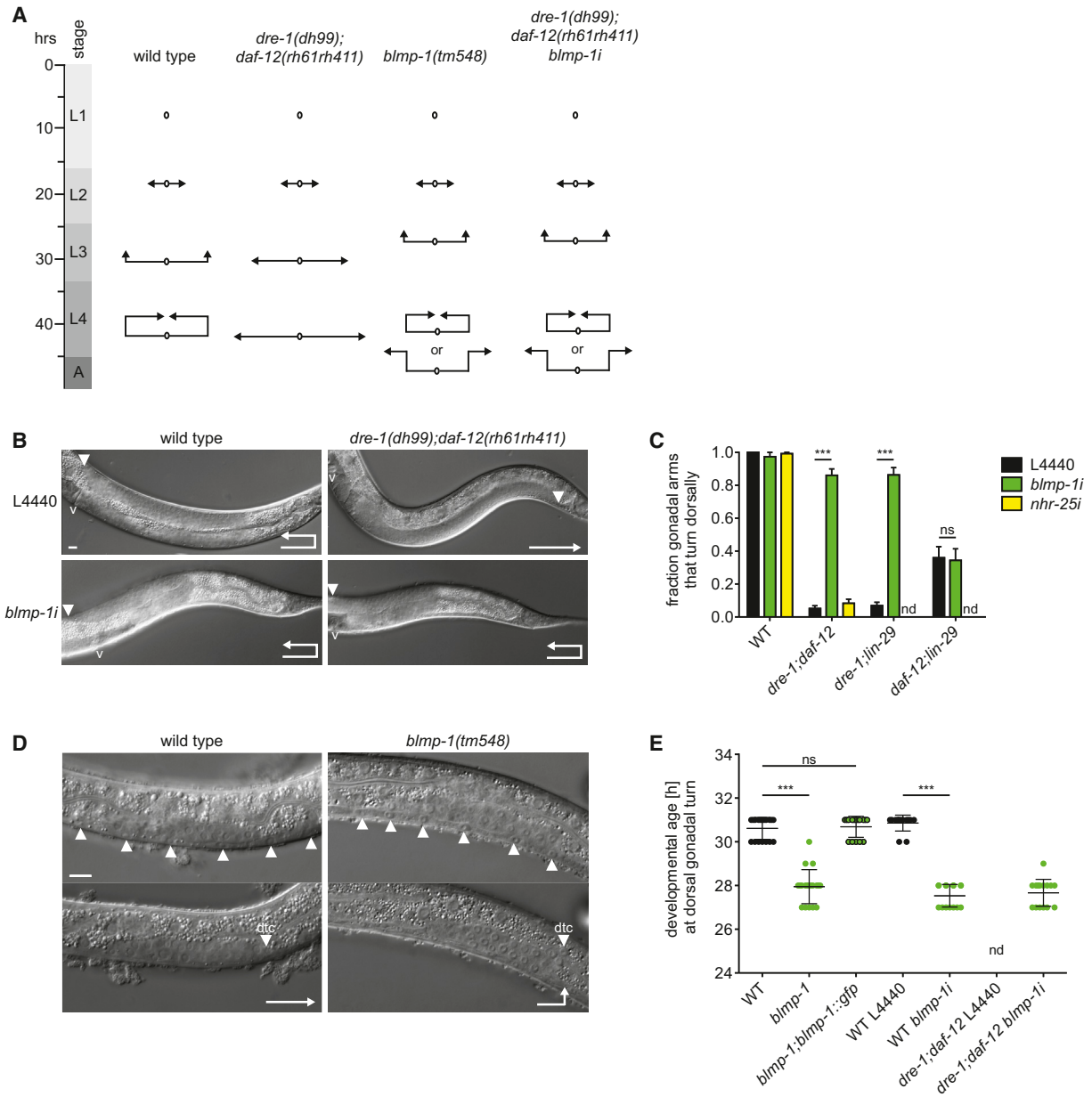

Figure 2. *blmp-1* Impedes Dorsal Migration of the Gonad

(A) Schematic representation of gonadal migration programs of WT worms and various mutants as inferred from inspection. Arrowheads indicate positions of the dtcs.

(B) Representative DIC images of WT and *dre-1;daf-12* young adult worms grown on L4440 empty vector control or *blmp-1* RNAi, respectively, showing one gonadal arm. Arrowheads indicate the position of the dtc. v, vulva.

(C) *blmp-1* depletion specifically suppresses gonadal migration defects of *dre-1;daf-12* and *dre-1;lin-29(n546)* mutants. ***p < 0.001 (ANOVA). Mean + SEM (n = 3, 40 gonadal arms each).

(D) Representative DIC images of 27 hr posthatching WT and *blmp-1* mutant larvae staged by the vulval precursor cells (arrowheads, upper panel). Dtcs migrate precociously in the *blmp-1* mutant (arrowheads, lower panel).

(E) dtcs turn dorsally ahead of time in *blmp-1* mutants, as well as in WT and *dre-1;daf-12* mutants, grown on *blmp-1* RNAi. ***p < 0.001 (ANOVA). Mean ± SD. ns, not significant; nd, not determined. Scale bars, 10 μm (B and D).

suggesting it acts downstream or parallel to these components (Figures 3A–3C; Figure S1A). In particular, *blmp-1*-retarded phenotypes (incomplete alae formation) largely prevailed over *hbl-1(ve18)*, *lin-42(n1089)*, and *lin-41i* precocious phenotypes, possibly closely linking these genes in a pathway (Figures 3A, 3C, and S1A). By comparison, suppression of hypomorphic *sop-2(bx91)* phenotypes was relatively weak, suggesting *blmp-1* might work upstream or in parallel to *sop-2* (Figure 3A). We interpret these interactions with caution, because not all alleles used were null.

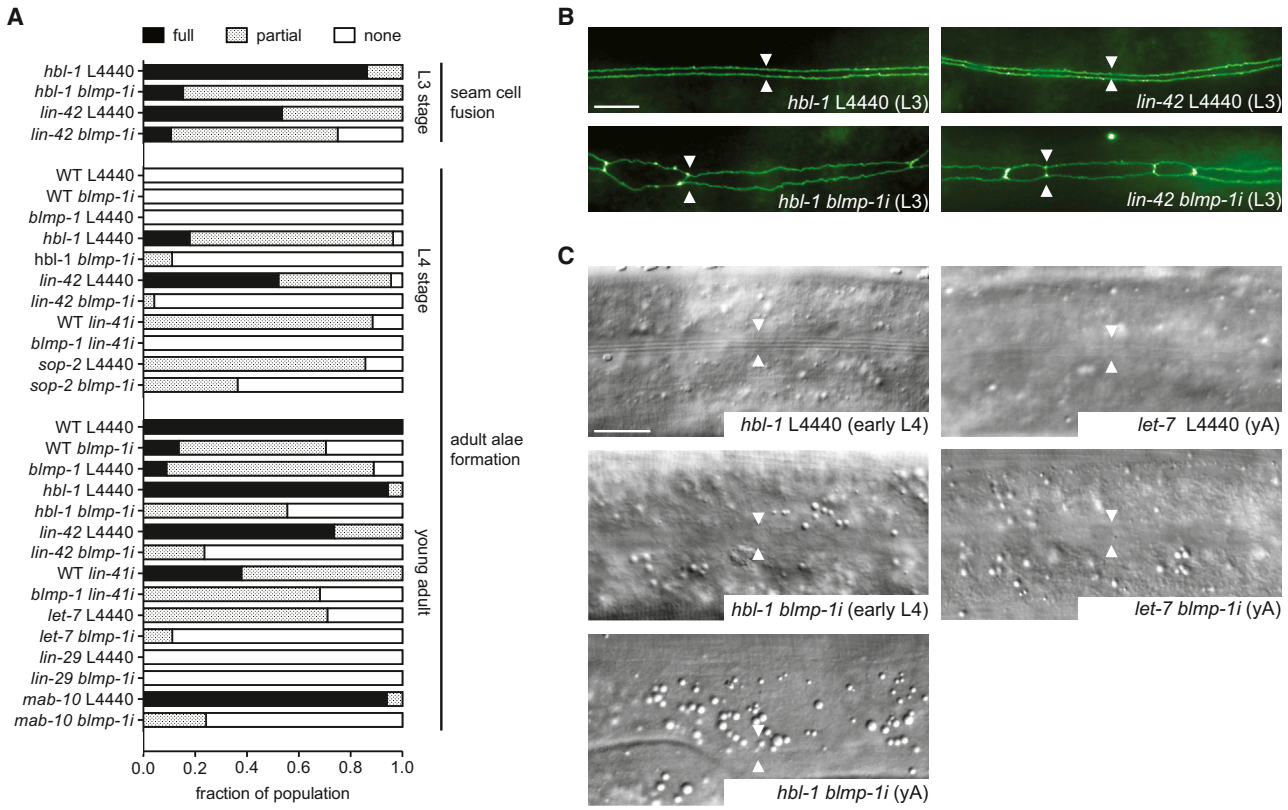

Figure 3. *blmp-1* Interacts with Precocious and Retarded Heterochronic Loci

(A) Epistasis and synergy experiments of *blmp-1(tm548)/blmp-1i* with precocious (*hbl-1(ve18)*, *lin-41i*, *lin-42(n1089)*, and *sop-2(bx91)*) and retarded (*let-7(n2853ts)*, *lin-29(n546)*, and *mab-10(e1248)*) heterochronic loci (n > 20). L4440 empty vector functions as control. Partial seam fusion refers to an incomplete seam syncytium with remaining unfused seam cells. Partial alae formation refers to poorly formed or incomplete adult alae. Temperature-sensitive alleles of *sop-2* and *let-7* were observed after shifting L1 larvae from 15°C to 23°C or 20°C, respectively.

(B) Representative pictures of seam cell adherence junctions as visualized by *ajm-1::gfp* in *hbl-1* and *lin-42* L3 larvae grown on L4440 empty vector control or *blmp-1* RNAi, respectively. Arrowheads indicate seam-seam boundaries.

(C) Representative DIC images of *hbl-1* and *let-7* mutants showing adult alae formation under control (L4440) and *blmp-1* depleted conditions at the early L4 or young adult (yA) stage. Arrowheads indicate positions of the seams.

Scale bars, 10 μm (B and C). See also Figure S1.

We next examined genetic interactions for synergy with various retarded heterochronic mutants working at the larval-to-adult transition. At this transition *hbl-1* and *lin-41* are downregulated posttranscriptionally by *let-7*/*let-7*-family microRNAs (Abbott et al., 2005; Abrahante et al., 2003; Slack et al., 2000). Consequentially, *lin-29*/EGR is derepressed and triggers adult-specific cell fates. Thus, *let-7* and *lin-29* loss of function cause retarded phenotypes: *let-7* mutants display incomplete seam cell fusion and poor or no adult alae; in *lin-29* mutants, both events fail entirely. RNAi-mediated knockdown of *blmp-1* in temperature-sensitive *let-7(n2853ts)* mutants slightly enhanced the *let-7*-retarded adult alae formation and the bursting phenotype at a semi-permissive temperature (Figures 3A and 3C; data not shown). No enhancement was detected for *lin-29(n546)* as its retarded phenotypes are fully penetrant (Figures 3A and S1B). The transcriptional cofactor *mab-10*/NAB cooperates with *lin-29*/EGR to specify the adult seam fate. Loss-of-function mutations of *mab-10* do not affect seam cell fusion and adult alae formation, but subsets of seam cells undergo an extra nuclear division after they fuse into the seam syncytium (Harris and Horvitz, 2011). *blmp-1* depletion enhanced the penetrance of the extra nuclear division phenotype of *mab-10(e1248)* (Figure S1C) and worms rarely formed adult alae (Figures 3A and S1B), suggesting that *blmp-1* acts downstream or in parallel to *mab-10*. Altogether, these analyses reveal a broad role for *blmp-1* as a developmental timing gene, promoting many aspects of seam cell terminal differentiation.

dre-1/blmp-1 Regulate the Life History of *C. elegans*

The interactions described above reveal that *dre-1* and *blmp-1* act in opposition for developmental timing events. We wondered whether this relationship also applied to other processes. Interestingly, we found that *blmp-1* and *dre-1* both function to regulate entry into the long-lived dauer stage, an alternate third larval stage triggered under harsh environmental conditions and food scarcity. In particular, *blmp-1* mutants were defective in dauer formation (Daf-d), whereas *dre-1* mutants constitutively formed dauer larvae (Daf-c) albeit at low levels, suggesting the two genes normally promote and prevent dauer formation, respectively (Figure 4A). Consistent with our previous data, the

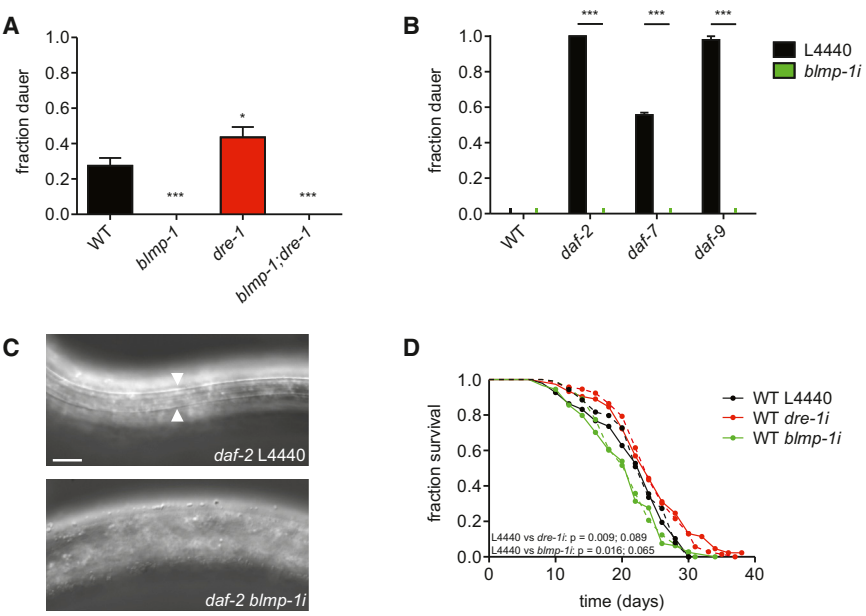

Figure 4. *dre-1* and *blmp-1* Show Opposite Phenotypes in Dauer Formation and Lifespan

(A) Dauer formation of WT, *dre-1(dh99)*, *blmp-1(tm548)*, and *dre-1(dh99);blmp-1(tm548)* animals scored on plates lacking cholesterol at 27°C. *p < 0.05, ***p < 0.001 (ANOVA). Mean + SEM (n ≥ 8, >100 worms each).

(B) Dauer formation of WT, *daf-2(e1368)*, *daf-7(e1372)*, and *daf-9(dh6)* animals scored on regular NGM plates at 25°C under control (L4440) or *blmp-1*-depleted conditions. In the latter genotypes, *blmp-1* depletion led to L3/L4 arrest without dauer alae and SDS resistance. ***p < 0.001 (ANOVA). Mean + SEM (n = 3, 15 worms each).

(C) Representative DIC images of *daf-2(e1368)* mutants grown on L4440 empty vector control or *blmp-1* RNAi at 25°C for 48 hr. Arrowheads indicate dauer alae. Scale bar, 10 μm.

(D) Lifespan analysis: WT animals were grown on RNAi from the L4 stage as indicated. Dashed lines represent an independent repeat of the experiment. First, given p value (Mantel-Cox log rank method) corresponds to the experiment displayed with solid lines.

blmp-1 mutant phenotype (Daf-d) prevailed in the double mutant (Figure 4A). *blmp-1* depletion also suppressed canonical Daf-c loci, *daf-2*/InsR, *daf-7*/TGFβ, and *daf-9*/CYP27A1 (Figures 4B and 4C), placing *blmp-1* downstream of insulin/IGF, TGFβ, and steroidal signaling at a late step in the dauer signaling pathways. In addition *blmp-1* and *dre-1* affected organismal lifespan. Knockdown of *blmp-1* from L4 onward shortened wild-type (WT) lifespan, similar to previous reports (Samuelson et al., 2007), whereas *dre-1* depletion resulted in a modest, but reproducible, lifespan increase (Figure 4D). Therefore, the two genes work in opposite ways for the life history traits of dauer formation and longevity.

Just as *blmp-1* loss suppressed *dre-1* phenotypes, *blmp-1* overexpression conversely further enhanced *dre-1* phenotypes: first, the *blmp-1* overexpressor evoked strongly retarded gonadal migration defects when grown on *dre-1* RNAi (Figure S2A). Second, it enhanced molting defects of *dre-1*-depleted worms (Figures S2B and S2C). Third, it was synthetic lethal in a *dre-1(dh99)* background, similar to *dre-1* null mutants. In sum, our genetic data reveal intimate genetic interaction between *dre-1* and *blmp-1* for multiple processes.

The SCF^{DRE-1} Complex Degrades BLMP-1 via the Proteasome

The genetic epistasis experiments described above place *blmp-1* downstream of *dre-1*, supporting the idea that BLMP-1 could be a substrate of the SCF^{DRE-1} E3-ubiquitin ligase. To directly test this hypothesis, we examined the effect of *dre-1* depletion on BLMP-1 protein levels. BLMP-1::GFP showed overlapping expression with DRE-1::GFP in seam and hypodermal cells as well as the dtcs (Figure S3A; data not shown). Consistent with a role in BLMP-1 proteolysis, we found that knockdown of *dre-1* resulted in a striking 7- to 8-fold increase in BLMP-1::GFP levels in seam and hypodermal cells (Figures 5A and 5B). Knockdown of other SCF complex components—the scaffold *cul-1* and the *skr-1* adaptor—also led to a substantial accumulation of BLMP-1::GFP, whereas knockdown of related molecules (*cul-4*, *skr-2*, and *-3*) had little or no effect (Figure 5B and S3B). In contrast, NHR-25::GFP expression showed no obvious *dre-1* dependence during L2 to L4 larval stages (Figure S3C). To test whether the UPS mediates BLMP-1 proteolysis, we inhibited the proteasome using the synthetic inhibitor bortezomib or *rpn-8* RNAi, which depletes a subunit of the proteasomal 19S cap. Both treatments significantly increased BLMP-1::GFP levels in seam and hypodermis (Figures 5C, 5D, and S3B).

We next analyzed endogenous BLMP-1 levels by western blotting using antibodies to visualize the native protein. In accord with our *blmp-1::gfp* transgene results, *dre-1* loss of function and proteasome inhibition by RNAi both resulted in a significant increase in endogenous BLMP-1 protein (Figures 5E and 5F). Whereas BLMP-1 levels were strongly elevated in a *dre-1(dh99)* mutant background, *blmp-1* mRNA levels were unchanged upon *dre-1* depletion or proteasome inhibition (Figures 5E–5G). These results further support the notion that the SCF^{DRE-1} complex posttranscriptionally regulates BLMP-1 through proteasome-mediated degradation.

If BLMP-1 were a direct substrate of DRE-1, then the two proteins would be predicted to physically interact. Therefore, we performed coimmunoprecipitation experiments in worms expressing DRE-1::GFP under its native promoter. We found that immunoprecipitation of DRE-1::GFP specifically coprecipitated a small fraction of endogenous BLMP-1 (<1% of input), whereas a NHR-25::GFP control did not (Figure 5H). When expressed in HEK293T cells under proteasome inhibition FLAG-HA-tagged DRE-1 specifically coprecipitated with 6xHis-tagged *C. elegans* BLMP-1, but not the closely related zinc-finger protein LIN-29 (Figure S3D). However, we could not detect ubiquitylation of *C. elegans* BLMP-1 in our assays (data not shown), but such species might be of low abundance or unstable in vivo and difficult to ubiquitylate in a heterologous system in vitro.

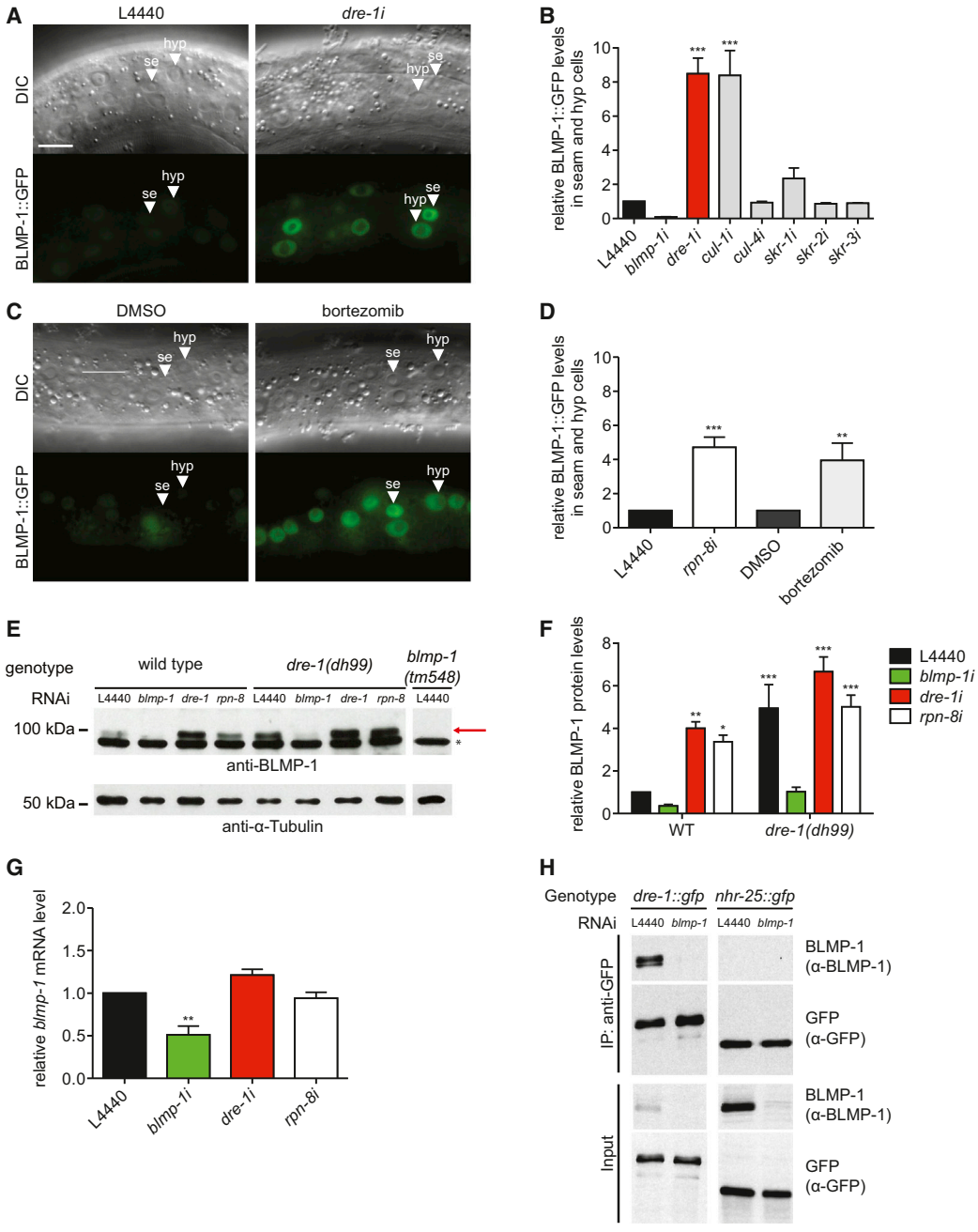

Figure 5. DRE-1 Targets BLMP-1 for Proteasomal Degradation

(A) Representative DIC and fluorescence images of BLMP-1::GFP expressing L4 larvae grown on L4440 empty vector control or *dre-1* RNAi.

(B) BLMP-1::GFP levels in seam and hypodermal cells are significantly increased upon *dre-1* and *cul-1* depletion. ***p < 0.001 (ANOVA). Mean + SEM (n ≥ 3, ≥10 cells of five worms each).

(C) Representative DIC and fluorescence images of BLMP-1::GFP expressing L4 larvae treated with 100 μM bortezomib or DMSO control.

(D) Proteasome inhibition (bortezomib and *rpn-8* RNAi) increases BLMP-1::GFP levels in seam and hypodermal cells. **p < 0.01, ***p < 0.001 (ANOVA). Mean + SEM (n ≥ 3, ≥10 cells of five worms each).

(E) Western blot analysis of endogenous BLMP-1 protein levels in WT, *dre-1*, and *blmp-1* L4 larvae after various RNAi treatments from the egg stage and onward. The asterisk marks a nonspecific band. The arrow points to the BLMP-1 band.

(F) Quantification of western blot analyses. *p < 0.05, **p < 0.01, ***p < 0.001 (ANOVA). Mean + SD (n = 5).

(G) qRT-PCR analysis of WT L4 larvae treated with the indicated RNAi from the egg stage. **p < 0.01 (ANOVA). Mean + SEM (n = 3).

(H) L3 larvae expressing integrated DRE-1::GFP or NHR-25::GFP as control were grown from the egg stage and onward on L4440 empty vector control or *blmp-1* RNAi-expressing bacteria, respectively, and utilized for anti-GFP immunoprecipitation (IP). Lysates and IP were analyzed by immunoblotting. Detected sizes: BLMP-1: ≈98 kDa, DRE-1::GFP: ≈145 kDa, and NHR-25::GFP: ≈120 kDa.

se, seam cell; hyp, hypodermal cell. Scale bars, 10 μm. See also Figures S2 and S3.

The DRE-1/BLMP-1 Interaction Is Conserved in Mammals

Importantly, the association of BLMP-1 with DRE-1 is evolutionarily conserved. First, like the worm proteins, human BLIMP-1 specifically coprecipitated with human FBXO11 when coexpressed in cultured HEK293T cells treated with proteasome inhibitor (Figures 6A and S4A). BLIMP-1 also weakly interacted with the closely related FBXO10, but not with other controls (Figure 6A). Interestingly, the ability to bind BLIMP-1 was substantially reduced when the Q491L amino acid substitution identified in the *Jeff* mouse mutant (Hardisty-Hughes et al., 2006) was introduced into human *FBXO11*, suggesting that the conserved region containing the point mutation may facilitate interaction (Figure 6A). Second, we found that immunopurified FBXO11 promoted BLIMP-1 ubiquitylation in vitro, dependent upon a functional F box domain, which tethers FBXO11 to the SCF complex: F box domain mutation (F box^{MUT}/V98A, C99A, and F102A) abolished binding to the SKP1 adaptor protein and consistently suppressed ubiquitylated BLIMP-1 higher molecular weight species (Figure 6B). Third, cycloheximide (CHX)-treated cells showed progressive proteolysis of worm or human BLMP-1/BLIMP-1 upon cotransfection of DRE-1/FBXO11, which strongly depended on a functional proteasome (Figures 6C and S4B). Rates of human BLIMP-1 proteolysis were significantly dampened by deletion of the FBXO11 F box domain (ΔF box) or by introducing the amino acid substitution FBXO11/Q491L (Figure 6C). Furthermore, inclusion of a deletion mutant, dominant-negative form of the SCF scaffold CUL1, but not other dominant-negative cullins, prevented FBXO11-dependent BLIMP-1 degradation (Figures S4C and S4D). In accord with a low BLIMP-1 binding affinity, FBXO10 overexpression slightly destabilized BLIMP-1 after CHX treatment (Figure 6C), indicating that FBXO10 might also harbor a minor capability to target BLIMP-1. Finally, in agreement with accelerated BLIMP-1 degradation, we found that short hairpin RNA (shRNA)-mediated depletion of FBXO11 in ARP1 multiple myeloma cells using two different shRNAs led to stabilization of endogenous BLIMP-1 in the presence of CHX (Figure 6D). Altogether, these experiments demonstrate that SCF^{FBXO11} mediates ubiquitin-mediated degradation of BLIMP-1, providing strong evidence for conserved proteolytic regulation across taxa.

BLMP-1 Is Dynamically Regulated in a Tissue-Specific Manner

Having established BLMP-1 as a DRE-1 substrate for proteolysis, we sought to better understand the dynamics of regulation in vivo. The genetic studies in *C. elegans* described above reveal that *blmp-1* acts at an intermediate step in dtc migration but promotes terminal differentiation in the hypodermis. To clarify the tissue-specific regulation of developmental timing by DRE-1/BLMP-1, we followed BLMP-1::GFP levels in these tissues throughout larval development.

In the dtcs, BLMP-1::GFP was expressed from mid-L2, when gonadal outgrowth initiates toward head and tail. By mid-L3 (28–30 hr developmental age [DA]), just prior to the dorsal gonadal turn, BLMP-1::GFP levels in the dtcs dropped dramatically (Figures 7A and 7B). Correlatively, DRE-1::GFP levels in the dtcs increased steadily from L2 to L4 (Figure S5A). In contrast, when worms were grown on *dre-1* RNAi, BLMP-1::GFP levels persisted to later ages and the dtcs frequently failed to turn dorsally (Figures 7A, 7B, and S2A). Our data therefore strongly suggest that timely DRE-1-mediated BLMP-1 degradation permits the gonadal turn, whereas high BLMP-1 levels in gonadal dtcs impede this event (Figure 7D).

Surprisingly, in seam and hypodermal cells BLMP-1::GFP levels were largely constant throughout larval development, except for a transient peak early in L4, which coincides with the time of seam cell fusion (Figure 7C), suggesting this BLMP-1 pulse could trigger the fusion event. Consistent with this, *dre-1* knockdown provoked a strong increase of seam and hypodermal BLMP-1::GFP expression earlier in development (Figure 7C), resulting in seam fusion as early as 28 hr of DA during the L3 stage. These observations are consistent with a model in which increased BLMP-1 levels initiate terminal differentiation events in the seams (Figure 7E). Unexpectedly, DRE-1::GFP levels in seam and hypodermis did not obviously change during this time (Figure S5B), implying that other instructive components or cofactors (e.g., a kinase or phosphatase) may contribute toward BLMP-1 regulation. Altogether, our data suggest that DRE-1 maintains a low steady-state level of BLMP-1 to prevent precocious terminal differentiation in the epidermis (Figure 7E).

blmp-1 Expression Profiles

To identify downstream effectors regulated by the transcription factor *blmp-1*, we performed RNA sequencing (RNA-seq) analysis of *blmp-1* mutant and WT animals harvested at the mid-L3 stage. We identified 325 significantly upregulated genes and 303 downregulated genes ($\geq$1.5-fold difference from WT, q value < 0.05) (Table S2). Differentially regulated genes included those enriched in the biological processes of molting and cuticle development, sugar and aminosugar metabolism, and protein modification (Figure 7F). The molting and cuticle-related regulated genes included *ptr-8*, *wrt-2*, *bed-3*, *nas-36*, and collagens (e.g., *col-7*, *col-91*, and *col-124*). *blmp-1*-dependent regulation of these genes was further confirmed by qRT-PCR in L3 larvae and young adult animals (Figure 7G). These data support the idea that *blmp-1* is a key regulator of *C. elegans* epidermal terminal differentiation.

DISCUSSION

In this study we discovered that the highly conserved SCF$^{DRE-1/FBXO11}$ E3-ubiquitin ligase complex targets the zinc-finger transcriptional repressor BLMP-1 as a substrate. DRE-1 and BLMP-1 work as a functional module to regulate not only *C. elegans* developmental timing but also the processes of dauer formation, molting, and longevity, revealing a global role in life history regulation. Remarkably, we find the DRE-1/BLMP-1 molecular interaction to be conserved in human cells, suggesting that FBXO11 and BLIMP-1 could act together to regulate related processes in mammals.

Multiple lines of evidence argue that BLMP-1/BLIMP-1 is an endogenous substrate degraded by the SCF$^{DRE-1/FBXO11}$ complex. First, BLMP-1 and DRE-1 coimmunoprecipitate in vivo from *C. elegans*, and, when expressed in cell culture, so do the human counterparts. Second, mammalian FBXO11 ubiquitylates BLIMP-1 in vitro. Third, BLMP-1 protein levels strikingly depend on the SCF^{DRE-1} complex and the proteasome. Loss of DRE-1

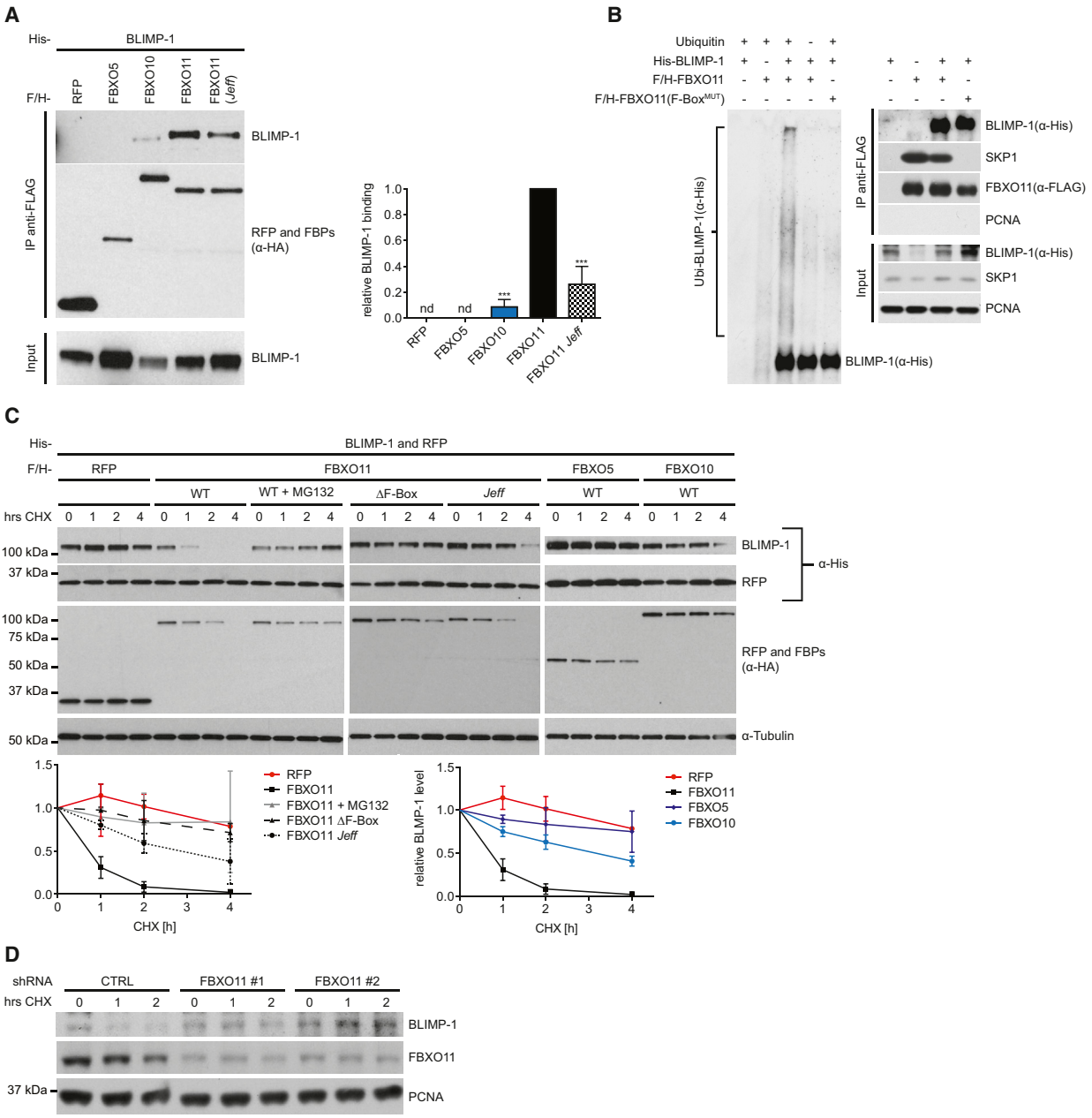

Figure 6. FBXO11 Directly Interacts with BLIMP-1 and Triggers Its Degradation

(A) Anti-FLAG IP of human FLAG-HA-tagged (F/H) RFP, -FBXO5, -FBXO10, -FBXO11, and -FBXO11(Q491L/*Jeff*) from HEK293T cells treated with 15 μM MG132. Human His-BLIMP-1 was coexpressed. See (C) for detected protein sizes. Quantification of RFP/F box-protein binding intensity to BLIMP-1 was normalized to BLIMP-1 input and FBXO11-BLIMP-1 association. ***$p < 0.001$ (ANOVA). Mean + SD (n = 5). nd, not detectable.

(B) HEK293T cells were transfected with His-tagged BLIMP-1, FLAG-tagged FBXO11, or -FBXO11(F box^{MUT}) and an empty vector as indicated. After immunopurification with anti-FLAG resin, in vitro ubiquitylation of BLIMP-1 was performed in the presence of E1 and E2s. Where indicated, ubiquitin was added. Samples were analyzed by immunoblotting (left panel). Immunoblots of whole-cell extracts and immunoprecipitations are shown in the right panel. Detected size of SKP1 is ≈19 kDa; the other proteins are as indicated in (C) and (D).

(C) Human BLIMP-1 stability was assessed in HEK293T cells transfected with His-BLIMP-1 and -RFP in combination with either F/H-tagged RFP, -FBXO11, -FBXO11 (ΔF box), -FBXO11(Q491L/*Jeff*), -FBXO5, or -FBXO10. Cells were treated with cycloheximide (CHX) or CHX ± 15 μM MG132 for 0, 1, 2, or 4 hr prior to harvesting and analysis by immunoblotting. Human BLIMP-1 stability was quantified from ≥3 independent experiments and normalized to coexpressed His-RFP. Mean + SD (n ≥ 3).

(D) Stability of endogenous BLIMP-1 was analyzed in ARP1 multiple myeloma cells infected with either viruses expressing two different FBXO11 shRNAs or an empty virus (CTRL) and selected for 72 hr. Cells were then treated with CHX for the indicated times, and protein extracts were analyzed by immunoblotting. The following sizes were detected: BLIMP-1 ≈90 kDA and FBXO11 ≈125 kDA.

See also Figure S4.

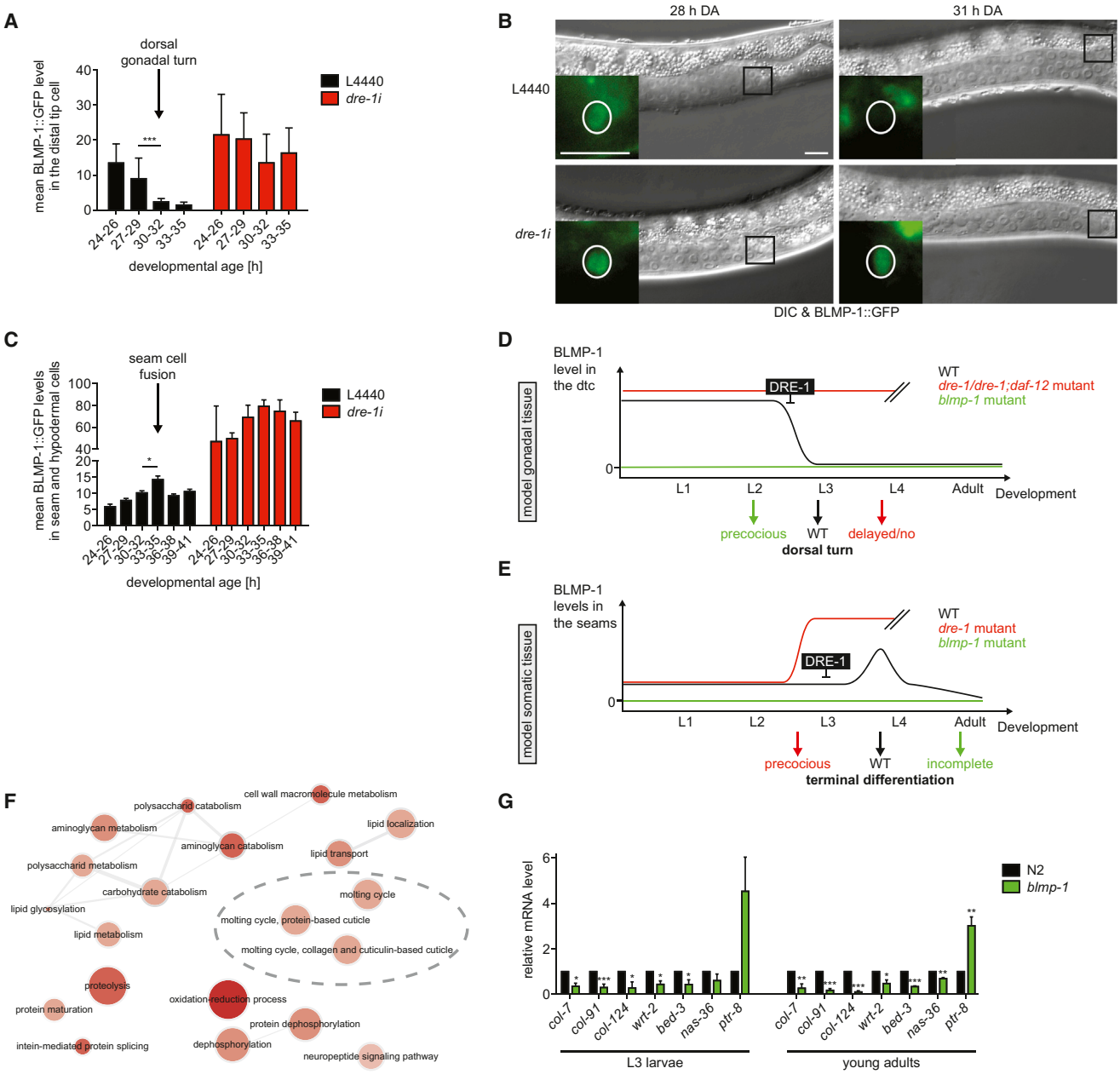

Figure 7. BLMP-1::GFP Levels Are Dynamically Regulated by DRE-1

(A) BLMP-1::GFP levels in the dtcs were assessed in ≥5 worms per grouped DA (developmental age). ***$p < 0.001$ (ANOVA). Mean + SD.

(B) Representative DIC images of age-matched L3 larvae, with zoom in on BLMP-1::GFP expression in the dtcs. Black box indicates the area enlarged in the fluorescence image. White circle roughly marks the dtc nucleus. Scale bars, 10 μm.

(C) BLMP-1::GFP levels in seam and hypodermal cells were assessed in ≥5 worms per grouped DA. *$p < 0.05$ (ANOVA). Mean + SEM.

(D) Model for *dre-1*/*blmp-1* action in gonadal tissue: BLMP-1 is downregulated in a *dre*-1-dependent manner in mid-L3 to allow the dorsal gonadal turn. In *dre-1* or *dre-1*/*daf-12* mutants BLMP-1 levels persist to later ages, leading to retarded migration defects, whereas the dorsal turn is preceded in the absence of BLMP-1.

(E) Somatic tissue: elevated BLMP-1 levels contribute to seam cell terminal differentiation, leading to precocious terminal differentiation in *dre-1* mutants and consequentially impaired terminal differentiation in the absence of BLMP-1. Double slashes indicate the end of data assessment.

(F) Summary of gene ontology (GO)/biological processes derived from DAVID analysis (Huang et al., 2009) of differentially regulated genes ($q < 0.05$, fold change > ±1.5) in WT versus *blmp-1* mutant animals from RNA sequencing data sets (n = 3). ReviGO was used for visualizing the resulting GO term classes and their semantic similarities (Supek et al., 2011). Bubble color, size, and line widths, respectively, indicate significance of enrichment, frequency of GO term in underlying data sets, and degree of similarity. More intense colors indicate a higher significance of enrichment.

(G) qRT-PCR analysis of *blmp-1*-regulated molting and cuticle-related genes in L3 larvae and young adult worms. *$p < 0.05$, **$p < 0.01$, ***$p < 0.001$ (t test). Mean + SEM (n ≥ 3).

See also Figure S5.

and other components of the SCF complex, as well as proteasome inhibition, result in elevated endogenous BLMP-1 or BLMP-1::GFP levels in *C. elegans*. Conversely, DRE-1 overexpression in cell culture enhances BLMP-1 degradation. This molecular function is conserved because mammalian FBXO11 degrades BLIMP-1 when expressed in cultured cells and shRNA-mediated depletion of FBOX11 in the ARP1 multiple myeloma cell line leads to stabilization of endogenous BLIMP-1. Finally, *blmp-1* depletion strongly suppresses *dre-1* heterochronic phenotypes in seam and gonadal tissue. This strict epistasis indicates that *dre-1* acts through *blmp-1* in a regulatory pathway and suggest that *dre-1* phenotypes arise largely from elevated BLMP-1 activity. In accord with this, *blmp-1* overexpression exacerbates *dre-1* phenotypes. Taken together, our results demonstrate that BLMP-1 is a substrate of the SCF^{DRE-1} complex and that this molecular activity is evolutionarily conserved. This study therefore provides critical evidence for BLMP-1/BLIMP-1 being specifically targeted for proteasomal degradation.

DRE-1 and BLMP-1 work as a module to regulate several aspects of *C. elegans* life history. In particular, our studies establish *dre-1*/*blmp-1* as key regulators of developmental timing within the heterochronic circuit during late larval development. Our previous work demonstrated that *dre-1* loss of function induces precocious seam cell fusion and synthetic retarded gonadal migration defects. Here, we discovered *blmp-1* depletion to efficiently suppress both phenotypes. On its own, *blmp-1* mutation leads to phenotypes opposite to *dre-1*, namely, retarded terminal differentiation of the seam cells (e.g., poor alae formation), on the one hand, and precocious migration of gonadal dtcs, on the other hand. These findings imply that *blmp-1* like its mammalian counterpart mediates terminal differentiation in some tissues but also controls intermediate stages of differentiation in others, presumably by regulating distinct targets. Importantly, *blmp-1* genetically interacts with multiple heterochronic loci that govern the larval-to-adult transition. *blmp-1* loss of function enhances retarded (*let-7*, *mab-10*/NAB) and suppresses precocious (*lin-41*/Trim71, *lin-42*/Period, *hbl-1*/Hunchback, and *sop-2*/PolycombG-like) heterochronic mutants for phenotypes in the epidermal seam cells. These interactions firmly place *blmp-1* within the heterochronic circuit controlling late larval development. Understanding how these genetic interactions translate into molecular regulatory events should be interesting to dissect in the future.

Many of the *C. elegans* heterochronic genes governing seam cell development have counterparts in mammals regulating skin stem cell homeostasis, including *blmp-1*/BLIMP-1 itself, *daf-12*/FXR/VDR, *lin-4*/*mir-125*, *let-7*, *lin-42*/Period, and others (Cianferotti et al., 2007; Horsley et al., 2006; Janich et al., 2011; Magnúsdóttir et al., 2007; Zhang et al., 2011). In particular, BLIMP-1 is required for terminal differentiation of the skin specifying the transition from granule to cornified layers in keratinocytes and stem cell lineages in the sebaceous gland (Horsley et al., 2006; Magnúsdóttir et al., 2007). Therein, BLIMP-1 and the vitamin D receptor were shown to be downregulated by *mir-125* to prevent skin stem cell differentiation (Zhang et al., 2011). Our data show that *C. elegans blmp-1* specifies terminal differentiation in the epidermis and indicate that this regulation could stem from *blmp-1*-dependent transcriptional changes in molting and cuticle synthesis genes. Moreover, dauer epistasis analyses place *blmp-1* at a late step in dauer morphogenesis pathways proximal to *daf-12*/FXR/VDR, bearing remarkable similarity to the mammalian situation in the skin. Interestingly, FBXO11 too is expressed in the skin (Hardisty-Hughes et al., 2006), suggesting a possible role for FBXO11 in BLIMP-1-dependent regulation of skin maturation.

Our studies also reveal that DRE-1/BLMP-1 affect organism-wide fates, including the entry into the dauer diapause, molting, and adult longevity. Moreover, *dre-1* was shown to function in male gonadal linker cell engulfment and *blmp-1* in male tail retraction (Chiorazzi et al., 2013; Nelson et al., 2011). Although much is known about vertebrate BLIMP-1, the rich signaling circuits presiding over *C. elegans* developmental timing, dauer signaling, molting, and lifespan might further inform mammalian stem cell progression and quiescence. In this view, it could be argued that the FBXO11/BLIMP-1 module not only acts as fate switch regulating cellular differentiation but also perhaps more broadly functions as part of a developmental timer across tissues and species.

Indeed, the notion that DRE-1/BLMP-1 comprise a conserved functional module may have several implications in mammals. Among other things, BLIMP-1 is a key regulator in primordial germ cell specification (Ohinata et al., 2005, 2009; Vincent et al., 2005), forelimb development, pharyngeal and heart morphogenesis (Vincent et al., 2005), T cell differentiation (Martins and Calame, 2008), pluripotency, and reprogramming (Nagamatsu et al., 2011). By inference, FBXO11 could work in tandem with BLIMP-1 in at least some of these contexts by controlling its turnover.

Despite its high conservation, relatively little is known about the biological function of mammalian FBXO11. Its loss of function is associated with chronic otitis media, facial clefting, and other developmental abnormalities (Hardisty et al., 2003; Hardisty-Hughes et al., 2006; Segade et al., 2006). Our studies suggest these phenotypes could in some measure result from aberrantly elevated BLIMP-1 levels, because FBXO11-dependent BLIMP-1 degradation is significantly impaired by introducing the FBXO11 *Jeff* mutation, which affects a highly conserved residue. FBXO11 is also known to play a critical role in tumorigenesis in the immune system. Duan et al. (2012) recently showed FBXO11 to target BCL6 for proteasomal degradation and FBXO11 inactivation results in aberrantly elevated BCL6 levels in diffuse large B cell lymphomas. Zinc-finger proteins BLIMP-1 and BCL6 are reciprocally antagonistic transcription factors that serve as a self-reinforcing switch to determine B- and T- cell fates (Crotty et al., 2010). Specifically, BLIMP-1 promotes terminal differentiation of B-plasma cells, whereas BCL6 functions in the maintenance of germinal center B cells. *Blimp-1* inactivation is also associated with the onset of B Cell-like diffuse large B cell lymphomas (Mandelbaum et al., 2010). Intriguingly, FBXO11 thus targets both BLIMP-1 (this work) and BCL6 for proteolytic degradation, but how their regulation is coordinated within normal immune lineages and in tumorigenesis is not yet understood. The closely related FBXO10 has also been implicated in degrading BCL2 (Chiorazzi et al., 2013), suggesting a general role for FBXO10/11 complexes in immune function. It is noteworthy that immune development, too, employs many homologs of developmental timing

genes, including *lin-4*, LIN28, and *let-7* modules (O'Connell et al., 2010; Yuan et al., 2012).

Taken together, we discovered BLMP-1 as a substrate of the SCF^{DRE-1} complex, modulating developmental timing, and other life history traits in *C. elegans*. Given the remarkable degree of structural and functional conservation of these two proteins, we hypothesize that the FBXO11/BLIMP-1 module could regulate metazoan cellular fate decisions across tissues.

EXPERIMENTAL PROCEDURES

C. elegans Strains, RNAi, and Treatments

C. elegans strains were grown under standard conditions at 20°C unless otherwise noted (Brenner, 1974). Strains used are listed in the Supplemental Experimental Procedures. RNAi treatment was performed as described (Kamath and Ahringer, 2003). In general, L4 larvae were moved to corresponding RNAi plates. RNAi clones were available from the Ahringer collection, except for *dre-1* RNAi, which we described previously (Fielenbach et al., 2007). Proteasome inhibition was achieved by transferring L3 larvae to a plate containing 100 μM bortezomib (in DMSO) on top of the bacteria lawn, for 6 hr.

Microscopy and Phenotype Analysis

Heterochronic phenotypes were analyzed at specific larval stages as assessed by gonad morphology and vulva formation. Nomarski differential interference contrast (DIC) microscopy was used to score seam cell number (*scm-1::gfp* marker), seam cell fusion (*ajm-1::gfp* marker), and adult alae formation, each on one side of individual animals. Worms were anesthetized with 1 mM levamisole. Fluorescence microscopy was performed on a Carl Zeiss Axio Imager Z1. GFP intensity in seam/hypodermal cells was leveled from 5–10 cells per animal, whereas for measurements in the dtc, one dtc per animal was analyzed. Fluorescence intensity was determined using the ImageJ software (http://rsbweb.nih.gov/ij/).

Dauer and Lifespan Analysis

For dauer assays worms were synchronized by egg-lay on OP50 or HT115 bacteria and scored after 48 hr (27°C) or 60 hr (25°C). Lifespan assays were performed at 20°C. Worms were synchronized by egg-lay and transferred to RNAi plates at the L4 stage. Worms undergoing internal hatching, bursting vulva, or crawling off the plates were censored.

Antibodies

The following antibodies were used in this study: BLMP-1 (rb, Novus Bio), GFP (ms, Clontech), α-tubulin (ms, Sigma), HA (rat, Roche), His (ms, QIAGEN; rb, Santa Cruz), FLAG (ms and rb, SIGMA), PCNA (ms, Invitrogen), BLIMP-1 (rb, ab59369, Abcam; ms, 3H2-E8, Novus Bio), FBXO11 (rb, NB100-59826, Novus Bio), and SKP1 (Pagano lab).

C. elegans Biochemistry

For the western blot analysis, synchronized L4 larvae were lysed in SDS sample buffer, and equal volumes were applied to SDS-PAGE and immunblotting. Band intensity was quantified with Adobe Photoshop.

For immunoprecipitation (IP) assays, eggs were isolated by bleach treatment. After a 3 hr hatching period, L1 larvae were washed off with M9 buffer and transferred to RNAi plates. L3 larvae were lysed in worm IP buffer (50 mM Tris/HCl [pH 7.4], 150 mM NaCl, 1 mM EDTA, 0.1% NP-40, protease and phosphatase inhibitor cocktail [Roche]) using a dounce homogenizer. Worm lysates were incubated with 40 μl GFP-Trap agarose beads (Chromotek) for 1 hr at 4°C and washed five times with worm washing buffer (same as worm IP buffer, but with 300 mM NaCl and 0.75% NP-40). Precipitants were eluted with SDS sample buffer and analyzed by SDS-PAGE and immunoblotting.

Cell Culture and IP Experiments

HEK293T cells were maintained in Dulbecco's modified Eagle's medium, supplemented with 10% fetal bovine serum (GIBCO). Transfections were performed using Lipofectamine 2000 (Invitrogen) in accordance with the manufacturer's instruction. Plasmid construction is described in the Supplemental Experimental Procedures. For IP experiments (not prior to ubiquitylation assay), cells were treated with 15 μM MG132 or DMSO control for 4 hr prior to harvesting. Cells were lysed 20 hr posttransfection in lysis buffer (50 mM Tris/HCl [pH 7.4], 120 mM NaCl, 0.5% NP-40, protease and phosphatase inhibitor cocktail [Roche]) and subsequently incubated with anti-FLAG-M2 resin (Sigma). Precipitated proteins were eluted by competition with 3xFLAG peptide (Sigma) and analyzed by immunoblotting. To study BLIMP-1 turnover, transfected cells were treated with 100 μg/ml cycloheximide (AppliChem) for the indicated time intervals 20 hr posttransfection. Cells were lysed in lysis buffer and analyzed by SDS-PAGE and immunoblotting. Whole-cell lysates and CHX treatment in ARP1 cells was performed as described (Duan et al., 2012).

Gene Silencing by shRNAs

Sequences of FBXO11 shRNAs were as follows: (1) GAGTTTACATCTTT GGTGA and (2) CAATTGTTCGGCATAACAA. shRNA lentiviruses were produced as described (Phan et al., 2007). ARP1 multiple myeloma cells were infected by resuspension in virus-containing supernatants and centrifugation. Twenty-four hours after infection, cells were resuspended in fresh medium and selected with puromycin.

In Vitro Ubiquitylation

HEK293T cells were cotransfected with His-BLIMP-1 and FLAG-FBXO11 or -FBXO11($F\ box^{MUT}$) and lysed using isotonic NP40 buffer with Turbonuclease (Accelagen). Lysates were precleared with 0.40 μm filters and FLAG-tagged complexes were isolated using anti-FLAG-M2 resin (Sigma). Complexes were eluted by competition with 3xFLAG peptide (Sigma).

In vitro ubiquitylation assays were performed in a volume of 30 μl containing 0.1 μM UBE1 (Boston Biochem), 10 ng/ml Ubch3, 10 ng/ml Ubch5c, 1 μM ubiquitin aldehyde, ±2.5 μg/μl ubiquitin (Sigma), and either SCF^{FBXO11} or $SCF^{FBXO11-F\ box-MUT}$ complex in a ubiquitylation buffer (50 mM Tris [pH 7.6], 2 mM ATP, 5 mM $MgCl_2$, 0.6 mM DTT, and okadaic acid 0.1 mM) for 45 min at 37°C.

Statistical Analysis

Statistical analyses were performed as indicated using GraphPad Prism (GraphPad software).

ACCESSION NUMBERS

The Gene Expression Omnibus NCBI accession number for the RNA-seq data of WT and *blmp-1* mutant L3 larvae reported in this paper is GSE55225.

SUPPLEMENTAL INFORMATION

Supplemental Information includes Supplemental Experimental Procedures, five figures, and two tables and can be found with this article online at http://dx.doi.org/10.1016/j.devcel.2014.01.028.

ACKNOWLEDGMENTS

We would like to thank members of the Antebi lab for scientific discussion and review of the manuscript and the *C. elegans* Genetic Center (CGC) at the University of Minnesota as well as the Japanese National Bioresource Project Knockout Consortium for strains. This work was supported by the Deutsche Forschungsgemeinschaft (DFG/SFB635 to C.G. and A.A.), the Max Planck Society (to A.A.), CECAD/DFG (to M.H.), and the National Institutes of Health (R01-GM057587, R37-CA076584, R21-CA161108, and R03 TW009040 to M.P.). M.P. is an investigator of the Howard Hughes Medical Institute.

Received: October 8, 2013
Revised: January 22, 2014
Accepted: January 28, 2014
Published: March 6, 2014

REFERENCES

Abbas, T., Mueller, A.C., Shibata, E., Keaton, M., Rossi, M., and Dutta, A. (2013). CRL1-FBXO11 promotes Cdt2 ubiquitylation and degradation and regulates Pr-Set7/Set8-mediated cellular migration. Mol. Cell *49*, 1147–1158.

Abbott, A.L., Alvarez-Saavedra, E., Miska, E.A., Lau, N.C., Bartel, D.P., Horvitz, H.R., and Ambros, V. (2005). The let-7 MicroRNA family members mir-48, mir-84, and mir-241 function together to regulate developmental timing in Caenorhabditis elegans. Dev. Cell *9*, 403–414.

Abrahante, J.E., Daul, A.L., Li, M., Volk, M.L., Tennessen, J.M., Miller, E.A., and Rougvie, A.E. (2003). The Caenorhabditis elegans hunchback-like gene lin-57/hbl-1 controls developmental time and is regulated by microRNAs. Dev. Cell *4*, 625–637.

Ambros, V., and Horvitz, H.R. (1984). Heterochronic mutants of the nematode Caenorhabditis elegans. Science *226*, 409–416.

Brenner, S. (1974). The genetics of Caenorhabditis elegans. Genetics *77*, 71–94.

Cai, Q., Sun, Y., Huang, X., Guo, C., Zhang, Y., Zhu, Z., and Zhang, H. (2008). The Caenorhabditis elegans PcG-like gene sop-2 regulates the temporal and sexual specificities of cell fates. Genetics *178*, 1445–1456.

Chiorazzi, M., Rui, L., Yang, Y., Ceribelli, M., Tishbi, N., Maurer, C.W., Ranuncolo, S.M., Zhao, H., Xu, W., Chan, W.-C.C., et al. (2013). Related F-box proteins control cell death in Caenorhabditis elegans and human lymphoma. Proc. Natl. Acad. Sci. USA *110*, 3943–3948.

Cianferotti, L., Cox, M., Skorija, K., and Demay, M.B. (2007). Vitamin D receptor is essential for normal keratinocyte stem cell function. Proc. Natl. Acad. Sci. USA *104*, 9428–9433.

Crotty, S., Johnston, R.J., and Schoenberger, S.P. (2010). Effectors and memories: Bcl-6 and Blimp-1 in T and B lymphocyte differentiation. Nat. Immunol. *11*, 114–120.

Duan, S.S., Cermak, L.L., Pagan, J.K.J., Rossi, M.M., Martinengo, C.C., di Celle, P.F.P., Chapuy, B.B., Shipp, M.M., Chiarle, R.R., and Pagano, M.M. (2012). FBXO11 targets BCL6 for degradation and is inactivated in diffuse large B-cell lymphomas. Nature *481*, 90–93.

Fielenbach, N., Guardavaccaro, D., Neubert, K., Chan, T., Li, D., Feng, Q., Hutter, H., Pagano, M., and Antebi, A. (2007). DRE-1: an evolutionarily conserved F box protein that regulates C. elegans developmental age. Dev. Cell *12*, 443–455.

Gissendanner, C.R., and Sluder, A.E. (2000). nhr-25, the Caenorhabditis elegans ortholog of ftz-f1, is required for epidermal and somatic gonad development. Dev. Biol. *221*, 259–272.

Hada, K., Asahina, M., Hasegawa, H., Kanaho, Y., Slack, F.J., and Niwa, R. (2010). The nuclear receptor gene nhr-25 plays multiple roles in the Caenorhabditis elegans heterochronic gene network to control the larva-to-adult transition. Dev. Biol. *344*, 1100–1109.

Hardisty, R.E., Erven, A., Logan, K., Morse, S., Guionaud, S., Sancho-Oliver, S., Hunter, A.J., Brown, S.D.M., and Steel, K.P. (2003). The deaf mouse mutant Jeff (Jf) is a single gene model of otitis media. J. Assoc. Res. Otolaryngol. *4*, 130–138.

Hardisty-Hughes, R.E., Tateossian, H., Morse, S.A., Romero, M.R., Middleton, A., Tymowska-Lalanne, Z., Hunter, A.J., Cheeseman, M., and Brown, S.D.M. (2006). A mutation in the F-box gene, Fbxo11, causes otitis media in the Jeff mouse. Hum. Mol. Genet. *15*, 3273–3279.

Harris, D.T., and Horvitz, H.R. (2011). MAB-10/NAB acts with LIN-29/EGR to regulate terminal differentiation and the transition from larva to adult in C. elegans. Development *138*, 4051–4062.

Horsley, V., O'Carroll, D., Tooze, R., Ohinata, Y., Saitou, M., Obukhanych, T., Nussenzweig, M., Tarakhovsky, A., and Fuchs, E. (2006). Blimp1 defines a progenitor population that governs cellular input to the sebaceous gland. Cell *126*, 597–609.

Huang, W., Sherman, B.T., and Lempicki, R.A. (2009). Systematic and integrative analysis of large gene lists using DAVID bioinformatics resources. Nat. Protoc. *4*, 44–57.

Janich, P., Pascual, G., Merlos-Suárez, A., Batlle, E., Ripperger, J., Albrecht, U., Cheng, H.-Y.M., Obrietan, K., Di Croce, L., and Benitah, S.A. (2011). The circadian molecular clock creates epidermal stem cell heterogeneity. Nature *480*, 209–214.

Kamath, R.S., and Ahringer, J. (2003). Genome-wide RNAi screening in Caenorhabditis elegans. Methods *30*, 313–321.

Magnúsdóttir, E., Kalachikov, S., Mizukoshi, K., Savitsky, D., Ishida-Yamamoto, A., Panteleyev, A.A., and Calame, K. (2007). Epidermal terminal differentiation depends on B lymphocyte-induced maturation protein-1. Proc. Natl. Acad. Sci. USA *104*, 14988–14993.

Mandelbaum, J., Bhagat, G., Tang, H., Mo, T., Brahmachary, M., Shen, Q., Chadburn, A., Rajewsky, K., Tarakhovsky, A., Pasqualucci, L., and Dalla-Favera, R. (2010). BLIMP1 is a tumor suppressor gene frequently disrupted in activated B cell-like diffuse large B cell lymphoma. Cancer Cell *18*, 568–579.

Martins, G., and Calame, K. (2008). Regulation and functions of Blimp-1 in T and B lymphocytes. Annu. Rev. Immunol. *26*, 133–169.

Nagamatsu, G., Kosaka, T., Kawasumi, M., Kinoshita, T., Takubo, K., Akiyama, H., Sudo, T., Kobayashi, T., Oya, M., and Suda, T. (2011). A germ cell-specific gene, Prmt5, works in somatic cell reprogramming. J. Biol. Chem. *286*, 10641–10648.

Nelson, M.D., Zhou, E., Kiontke, K., Fradin, H., Maldonado, G., Martin, D., Shah, K., and Fitch, D.H.A. (2011). A bow-tie genetic architecture for morphogenesis suggested by a genome-wide RNAi screen in Caenorhabditis elegans. PLoS Genet. *7*, e1002010.

O'Connell, R.M., Rao, D.S., Chaudhuri, A.A., and Baltimore, D. (2010). Physiological and pathological roles for microRNAs in the immune system. Nat. Rev. Immunol. *10*, 111–122.

Ohinata, Y., Payer, B., O'Carroll, D., Ancelin, K., Ono, Y., Sano, M., Barton, S.C., Obukhanych, T., Nussenzweig, M., Tarakhovsky, A., et al. (2005). Blimp1 is a critical determinant of the germ cell lineage in mice. Nature *436*, 207–213.

Ohinata, Y., Ohta, H., Shigeta, M., Yamanaka, K., Wakayama, T., and Saitou, M. (2009). A signaling principle for the specification of the germ cell lineage in mice. Cell *137*, 571–584.

Park, S.W., Lee, S.-T., Sohn, Y.B., Cho, S.Y., Kim, S.-H., Kim, S.J., Kim, C.H., Ko, A.-R., Paik, K.-H., Kim, J.-W., and Jin, D.K. (2012). LIN28B polymorphisms are associated with central precocious puberty and early puberty in girls. Korean J. Pediatr. *55*, 388–392.

Phan, R.T., Saito, M., Kitagawa, Y., Means, A.R., and Dalla-Favera, R. (2007). Genotoxic stress regulates expression of the proto-oncogene Bcl6 in germinal center B cells. Nat. Immunol. *8*, 1132–1139.

Resnick, T.D., McCulloch, K.A., and Rougvie, A.E. (2010). miRNAs give worms the time of their lives: small RNAs and temporal control in Caenorhabditis elegans. Dev. Dyn. *239*, 1477–1489.

Rossi, M., Duan, S., Jeong, Y.-T., Horn, M., Saraf, A., Florens, L., Washburn, M.P., Antebi, A., and Pagano, M. (2013). Regulation of the CRL4(Cdt2) ubiquitin ligase and cell-cycle exit by the SCF(Fbxo11) ubiquitin ligase. Mol. Cell *49*, 1159–1166.

Rougvie, A.E., and Ambros, V. (1995). The heterochronic gene lin-29 encodes a zinc finger protein that controls a terminal differentiation event in Caenorhabditis elegans. Development *121*, 2491–2500.

Rybak, A., Fuchs, H., Hadian, K., Smirnova, L., Wulczyn, E.A., Michel, G., Nitsch, R., Krappmann, D., and Wulczyn, F.G. (2009). The let-7 target gene mouse lin-41 is a stem cell specific E3 ubiquitin ligase for the miRNA pathway protein Ago2. Nat. Cell Biol. *11*, 1411–1420.

Samuelson, A.V., Carr, C.E., and Ruvkun, G. (2007). Gene activities that mediate increased life span of C. elegans insulin-like signaling mutants. Genes Dev. *21*, 2976–2994.

Segade, F., Daly, K.A., Allred, D., Hicks, P.J., Cox, M., Brown, M., Hardisty-Hughes, R.E., Brown, S.D.M., Rich, S.S., and Bowden, D.W. (2006). Association of the FBXO11 gene with chronic otitis media with effusion and recurrent otitis media: the Minnesota COME/ROM Family Study. Arch. Otolaryngol. Head Neck Surg. *132*, 729–733.

Shaye, D.D., and Greenwald, I. (2011). OrthoList: a compendium of C. elegans genes with human orthologs. PLoS ONE *6*, e20085.

Silhánková, M., Jindra, M., and Asahina, M. (2005). Nuclear receptor NHR-25 is required for cell-shape dynamics during epidermal differentiation in Caenorhabditis elegans. J. Cell Sci. *118*, 223–232.

Skaar, J.R., Pagan, J.K., and Pagano, M. (2013). Mechanisms and function of substrate recruitment by F-box proteins. Nat. Rev. Mol. Cell Biol. *14*, 369–381.

Slack, F.J., Basson, M., Liu, Z., Ambros, V., Horvitz, H.R., and Ruvkun, G. (2000). The lin-41 RBCC gene acts in the C. elegans heterochronic pathway between the let-7 regulatory RNA and the LIN-29 transcription factor. Mol. Cell *5*, 659–669.

Sulston, J.E., and Horvitz, H.R. (1977). Post-embryonic cell lineages of the nematode, Caenorhabditis elegans. Dev. Biol. *56*, 110–156.

Supek, F., Bošnjak, M., Škunca, N., and Šmuc, T. (2011). REVIGO summarizes and visualizes long lists of gene ontology terms. PLoS ONE *6*, e21800.

Tennessen, J.M., Gardner, H.F., Volk, M.L., and Rougvie, A.E. (2006). Novel heterochronic functions of the Caenorhabditis elegans period-related protein LIN-42. Dev. Biol. *289*, 30–43.

Tunyaplin, C., Shapiro, M.A., and Calame, K.L. (2000). Characterization of the B lymphocyte-induced maturation protein-1 (Blimp-1) gene, mRNA isoforms and basal promoter. Nucleic Acids Res. *28*, 4846–4855.

Turner, C.A., Jr., Mack, D.H., and Davis, M.M. (1994). Blimp-1, a novel zinc finger-containing protein that can drive the maturation of B lymphocytes into immunoglobulin-secreting cells. Cell *77*, 297–306.

Vincent, S.D., Dunn, N.R., Sciammas, R., Shapiro-Shalef, M., Davis, M.M., Calame, K., Bikoff, E.K., and Robertson, E.J. (2005). The zinc finger transcriptional repressor Blimp1/Prdm1 is dispensable for early axis formation but is required for specification of primordial germ cells in the mouse. Development *132*, 1315–1325.

Yu, J., Vodyanik, M.A., Smuga-Otto, K., Antosiewicz-Bourget, J., Frane, J.L., Tian, S., Nie, J., Jonsdottir, G.A., Ruotti, V., Stewart, R., et al. (2007). Induced pluripotent stem cell lines derived from human somatic cells. Science *318*, 1917–1920.

Yuan, J., Nguyen, C.K., Liu, X., Kanellopoulou, C., and Muljo, S.A. (2012). Lin28b reprograms adult bone marrow hematopoietic progenitors to mediate fetal-like lymphopoiesis. Science *335*, 1195–1200.

Zhang, L., Stokes, N., Polak, L., and Fuchs, E. (2011). Specific microRNAs are preferentially expressed by skin stem cells to balance self-renewal and early lineage commitment. Cell Stem Cell *8*, 294–308.